nature geoscience

LETTERS

PUBLISHED ONLINE: 2 NOVEMBER 2015 | DOI: 10.1038/NGEO2569

Mantle flow geometry from ridge to trench beneath the Gorda–Juan de Fuca plate system

Robert Martin-Short[1]*, Richard M. Allen[1], Ian D. Bastow[2], Eoghan Totten[1,2] and Mark A. Richards[1]

Tectonic plates are underlain by a low-viscosity mantle layer, the asthenosphere. Asthenospheric flow may be induced by the overriding plate or by deeper mantle convection[1]. Shear strain due to this flow can be inferred using the directional dependence of seismic wave speeds—seismic anisotropy. However, isolation of asthenospheric signals is challenging; most seismometers are located on continents, whose complex structure influences the seismic waves en route to the surface. The Cascadia Initiative, an offshore seismometer deployment in the US Pacific Northwest, offers the opportunity to analyse seismic data recorded on simpler oceanic lithosphere[2]. Here we use measurements of seismic anisotropy across the Juan de Fuca and Gorda plates to reconstruct patterns of asthenospheric mantle shear flow from the Juan de Fuca mid-ocean ridge to the Cascadia subduction zone trench. We find that the direction of fastest seismic wave motion rotates with increasing distance from the mid-ocean ridge to become aligned with the direction of motion of the Juan de Fuca Plate, implying that this plate influences mantle flow. In contrast, asthenospheric mantle flow beneath the Gorda Plate does not align with Gorda Plate motion and instead aligns with the neighbouring Pacific Plate motion. These results show that asthenospheric flow beneath the small, slow-moving Gorda Plate is controlled largely by advection due to the much larger, faster-moving Pacific Plate.

The Juan de Fuca plate system is the northernmost section of the Farallon slab, which is approaching complete subduction beneath the North American continent[3]. The system is subdivided into the Explorer, Juan de Fuca and Gorda segments, which subduct at $\sim$12 mm yr^{-1} in a $\sim$N60 °E direction beneath the Cascadia arc[4,5]. The assemblage is undergoing rollback at $\sim$24 mm yr^{-1} (ref. 4) and rotating clockwise as the Mendocino Triple Junction (MTJ) migrates northwards[4].

Questions about the mantle flow geometry beneath Cascadia focus on interaction between oceanic asthenosphere and the subducting slab[6]. Shear wave splitting, a technique that quantifies the magnitude and direction of seismic anisotropy, can address such questions[6,7]. Seismic anisotropy in the mantle develops owing to the lattice-preferred orientation (LPO) of various minerals[8]. Olivine, the main component of the upper mantle, is highly anisotropic[8,9]. Simple shearing under typical asthenosphere conditions yields olivine crystal alignment, with fast axes corresponding to the shearing direction[8]. Shear waves traversing such a medium are split into two orthogonal components, one of which is polarized in the fast direction. A delay time (δt) proportional to the strength and layer thickness of the anisotropy is acquired as the components transit the layer. The fast axis direction (ϕ) is used to determine the shearing direction and by inference the mantle flow geometry[7].

Onshore studies in Cascadia reveal uniformly trench-perpendicular anisotropy, indicative of sub-slab mantle flow[4,5]. Cascadia is unusual; most subduction zones demonstrate trench-parallel splitting[6]. This has been variously interpreted as rollback-induced flow[6], the influence of B-type olivine LPO in the mantle wedge[9], or the consequence of strong radial anisotropy in steeply dipping, entrained flow[10].

We analyse data from Cascadia Initiative seismometer deployments[2], including 27 onshore Transportable Array sites and 70 ocean-bottom seismometers (OBS), deployed in ten-month phases at 160 sites[2]. We analyse OBS data from years 1–3 of the Cascadia Initiative and 4 years of records from the NEPTUNE cabled seafloor observatory[11]. Public data from the X9 OBS array, deployed along the Blanco Fracture Zone in 2012–2013 (ref. 2) are also used (Supplementary Section 2).

Splitting parameters ϕ and δt are determined for each station–event pair using two open-source software packages, before results are stacked to produce a single measurement at each site (see Methods). Shear wave splitting with OBS data is challenging owing to high noise levels within the S frequency band[12,13] and uncertainty in instrument orientation[14]. We generally obtain 1–4 good-quality measurements per offshore station, compared with 8–15 results for the onshore sites (Supplementary Sections 3–6).

The Transportable Array stations produce a uniform splitting pattern along the length of the subduction zone (Fig. 1). The mean fast direction and delay times are N72° E and 1.34 s respectively, in agreement with previous studies and sub-parallel to the subduction direction of N60° E (refs 4,5). Offshore stations on the Juan de Fuca Plate exhibit a more complicated pattern: except for a single, ridge-parallel result near Cobb Hotspot, fast splitting directions (FSDs) vary between the trench-perpendicular and absolute plate motion (APM) direction. Alignment with the Juan de Fuca APM direction increases towards the trench (Fig. 2). The FSDs then rotate into the subduction direction as one moves onshore.

Sites on the Gorda Plate produce a highly uniform pattern, but are aligned with neither Gorda APM nor the subduction direction. Their mean FSD of N66° W aligns with the motion of the Pacific Plate ($\sim$N57° W; ref. 4) and with the ridge-perpendicular orientation ($\sim$N67° W). A marked change in FSD is observed just east of the trench in this region, where the fast directions rotate approximately 70° into a trench-perpendicular orientation (Fig. 2a). Results from stations situated on the Pacific Plate align well with APM, featuring a mean direction of N60° W.

This study complements previous shear wave splitting results from ocean basins[15,16] and enhances coverage of the region. A notable feature of the existing onshore pattern is the arcuate splitting geometry observed south of the MTJ in northern California, which

[1]McCone Hall, Department of Earth and Planetary Science, UC Berkeley, California 94720, USA. [2]Department of Earth Science and Engineering, Royal School of Mines, Prince Consort Road, Imperial College London, London SW7 2BP, UK. *e-mail: rmartin-short@berkeley.edu

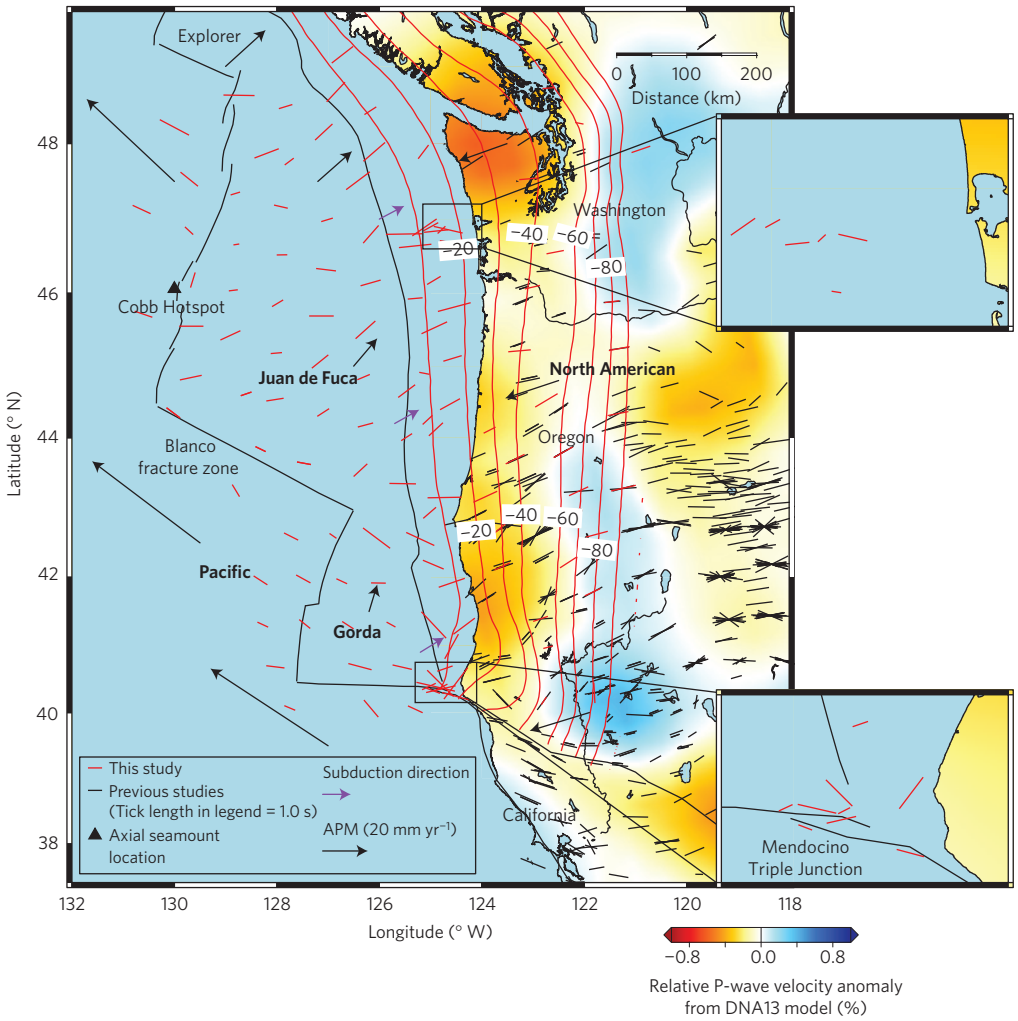

Figure 1 | Stacked splitting results determined by this study (red bars) and previous work (black bars; from refs 4,28). The displayed tomography is a 100–400 km vertical average through the DNA13 P-wave velocity model of ref. 29. This depth range corresponds to that part of the asthenosphere considered most likely to be the source of the observed anisotropy[9]. All splits are plotted at onshore seismometer/OBS locations. The splitting delay times are indicated by the length of the bars; example results with a delay time of 1.0 s are shown in the legend (bottom left). Black lines indicate plate boundaries, and the red lines are slab depth contours spaced at 10 km intervals[30]. Black arrows show the direction and magnitude of absolute plate motion (APM) in a hotspot reference frame[23], and purple arrows show the subduction direction[4]. Inset maps show regions featuring a high concentration of splitting results.

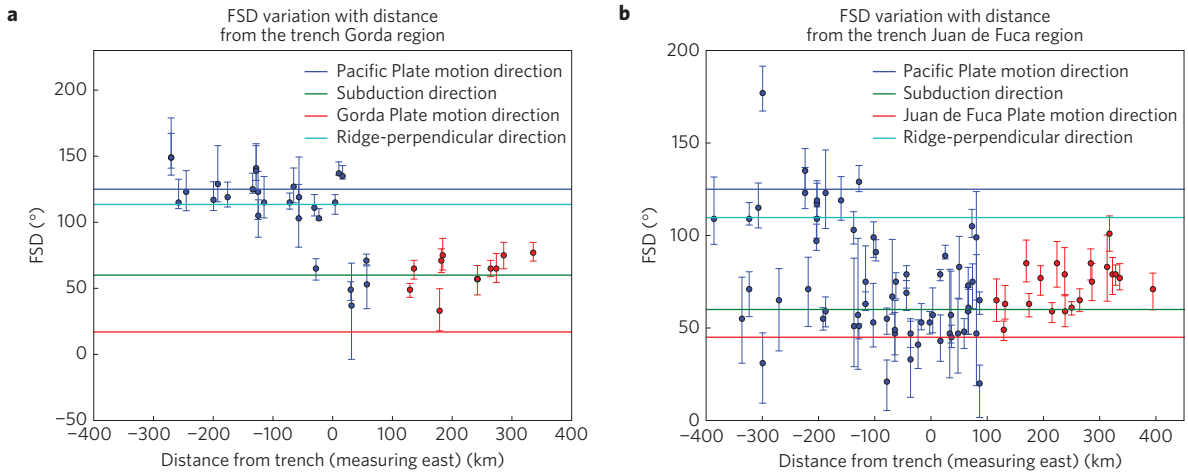

Figure 2 | Two distinct patterns in the variation of FSDs with distance from the trench. a, Results with latitudes between the MTJ and the southern tip of the Blanco Fracture Zone. **b**, Sites between latitudes of the southern and northern tips of the Juan de Fuca Ridge. In **a**, one population of FSDs lies west of the trench and is aligned with Pacific Plate motion, and another aligns with the subduction direction. Part **b** shows continuous variation in FSD with trench distance. Blue and red markers indicate offshore and onshore results, respectively. Error bars indicate the 95% confidence interval.

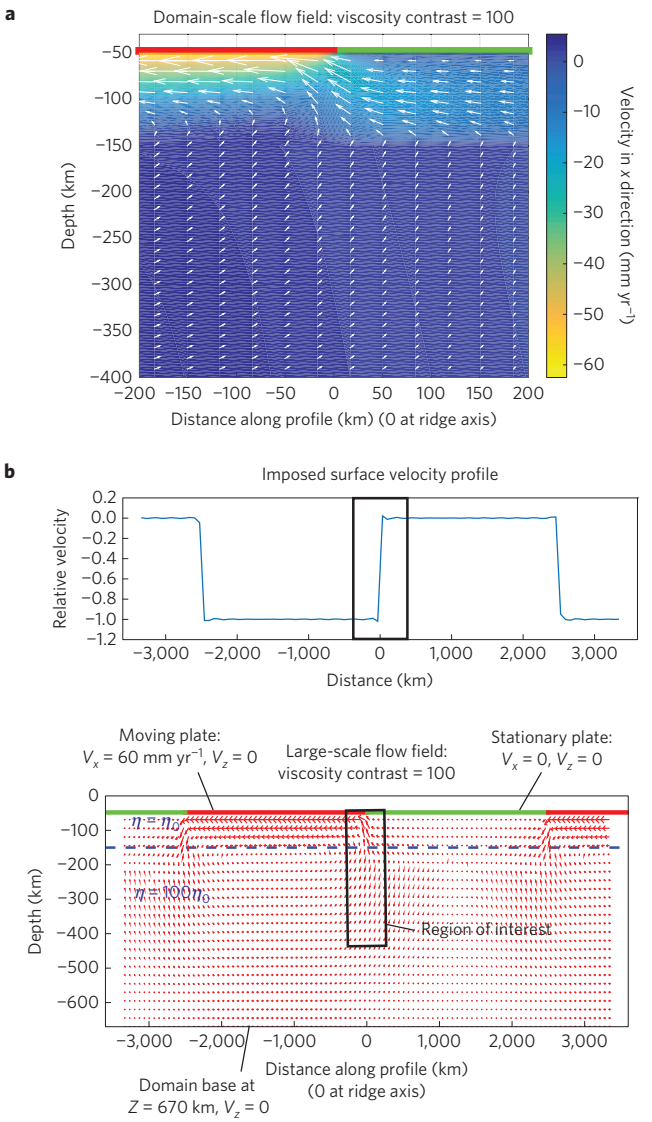

Figure 3 | Two-dimensional modelling to simulate mantle flow below the Gorda Plate as induced by motion of the Pacific Plate. The green plate is stationary while the red plate moves to the left at 60 mm yr^{-1}. This approximates the situation in profile perpendicular to the Gorda Ridge (see Methods for more detail). The set-up consists of an 'asthenosphere' from 50–150 km and a 'mesosphere' below. **a**, In our preferred model, the viscosity of the mesosphere is 100 times that of the asthenosphere. **b**, Details of the model set-up, including the imposed periodic surface velocity field, region of interest and large-scale induced flow structure. The motion of the red plate is seen to generate flow beneath the adjacent stationary plate.

follows the southern edge of the down-going Gorda slab[4,17] (Fig. 1). The subducting slab is imaged by body wave tomography as a segmented, high-velocity anomaly with a 'gap' beneath northern Oregon[18]. This 'gap' does not seem to influence the splitting pattern, however.

Limited back-azimuthal coverage makes it difficult to model dipping or multi-layer regional anisotropy in our study. We follow previous teleseismic splitting studies[4,5] of this area in interpreting a single anisotropic layer.

On oceanic plates, the dominant splitting signal is likely to arise from a combination of fossil anisotropy in the lithosphere and viscous shearing of the asthenosphere by plate motion[7]. According to the model of ref. 19, the lithospheric component should lie in the fossil spreading direction, and the asthenospheric component should align with the direction of present-day mantle flow. Both are parallel to the spreading direction close to mid-ocean ridges, but diverge beneath older lithosphere as the asthenosphere is dragged into the APM direction[19]. Shear wave splitting studies of the East Pacific Rise[15] and in French Polynesia[16] generally support this idea.

Given realistic estimates of 50 km, 4% and 4.6 km s^{-1} for the thickness, percentage anisotropy, and shear wave velocity for the Juan de Fuca Plate, respectively, a lithospheric splitting time contribution of 0.43 s is predicted[4,7]. This is significantly smaller than the OBS splitting times, implying that the asthenosphere is an important source of anisotropy.

The rotation of FSDs into the APM orientation east of the Juan de Fuca Ridge implies the influence of competing flow components. A variety of anisotropic fabrics might be expected in the vicinity of a mid-ocean ridge: upwelling asthenosphere in response to passive spreading, oriented melt pocket anisotropy along the ridge itself due to dyke intrusion[20], lateral flow away from the ridge[21] and basal drag fabrics as the plate moves away from the ridge[19].

Splitting directions close to the Juan de Fuca Ridge generally lie between the APM and ridge-perpendicular direction, suggesting that lateral flow and basal drag are the strongest influences. We do not see a concentration of null results at stations located close to the ridge (see Methods), suggesting that the influence of vertically oriented LPO due to upwelling is minimal or confined to a narrow region.

One exception to the pattern occurs at site J39, just east of Axial Seamount. The splitting parameters here are well constrained and suggest strong ridge-parallel anisotropy (Supplementary Section 7). This may be the result of aligned pockets of melt present near the ridge axis as observed on land in Ethiopia, a subaerial region of incipient oceanic spreading[20].

On the Gorda section of the plate system there is no significant variation in FSD with distance from the ridge. The FSDs are instead well aligned with the direction of Pacific Plate motion and with results from the Pacific Plate west of the Gorda Ridge and south of the Mendocino Fracture Zone. This implies that asthenospheric flow beneath the Gorda Plate, west of the trench, is determined by the regional pattern of shearing induced by the northwestward motion of the Pacific Plate, which moves at ~60 mm yr^{-1} (ref. 22). An alternative suggestion posits that because flow in this region is ridge perpendicular, it is driven primarily by spreading of the Gorda Ridge. This is less likely given the apparent limited influence of the faster-spreading Juan de Fuca Plate on the splitting pattern to the north. The splitting geometry on Gorda does not suggest major contributions from motion of the plate itself or rollback of the trench, which operates at less than half the speed of the Pacific Plate.

The uniform, subduction-parallel splitting pattern seen on the North American Plate east of the trench is interpreted as a consequence of entrained mantle material beneath the down-going slab. Fossil anisotropy in the continental lithosphere and subducted slab has been shown to be insufficient to explain the observed high delay times[4], thus implying an asthenospheric source[4]. Furthermore, the mantle wedge is thin or non-existent within most of the study area, so the only region thick enough to produce delay times commensurate to those observed is the sub-slab mantle[3,4]. Nevertheless, onshore FSDs tend towards North American APM at great distances from the trench (Fig. 2b), suggesting some influence from plate-motion-induced flow in the mantle wedge, or from lithospheric anisotropy. There is no significant change in delay times, however (Supplementary Section 8).

Immediately east of the trench of the Juan de Fuca Plate, splitting geometry rotates smoothly from an APM-parallel direction into a trench-perpendicular direction. This is indicative of entrained

easterly flow beneath the slab. In contrast, across the Gorda–North America plate boundary there is a sharp change in FSD (Fig. 2a). This is difficult to justify with a single-layer interpretation because it would imply marked changes in flow direction. Instead, this region could host two layers of mantle flow: a shallow layer induced by motion of the Pacific Plate and a deeper layer related to entrainment by the subducting slab.

Our observation provides a test for the models of refs 1,23, which suggest that plates moving slower than 40 mm yr^{-1} (ref. 23) and within 500 km of a constructive plate margin[1] are less able to influence asthenospheric flow. Both Gorda and Juan de Fuca meet these criteria, so the observation that Juan de Fuca does affect the asthenosphere perhaps sets lower bounds on the age and speed of a tectonic plate that can induce asthenospheric flow.

The Gorda Plate is young (<10 Myr; ref. 24), has a low absolute velocity[22], is undergoing internal deformation[24] and may have had its current APM for less than 2 Myr (ref. 24). In contrast, the neighbouring Pacific Plate is large, intact and fast moving. We have constructed a two-dimensional model of this situation using the method of ref. 25 to show that Pacific Plate motion is capable of generating westward flow beneath the width of the Gorda Plate, assuming that flow is largely confined to the uppermost mantle within a thin, low-viscosity asthenosphere (viscosity contrast 100, channel thickness 100 km (ref. 26)—see Methods) beneath Gorda. This simple model demonstrates the plausibility of our interpretation of the splitting pattern (Fig. 3).

This leads to discussion of the arcuate spitting geometry observed south of the MTJ and interpreted as flow forced eastwards around the slab edge by rollback[4]. This pattern, however, could be asthenospheric flow induced by drag from the N60° W drifting Pacific Plate. A larger-scale arcuate splitting pattern, situated much further east, may instead be the result of deep toroidal flow around the slab edge, which extends below 400 km in this region[17] (Supplementary Section 9).

In summary, we propose that the splitting observed on the Juan de Fuca plate system is mainly the result of APM-driven asthenosphere flow. At depth, below the Cascada fore-arc, the down-going slab entrains underlying mantle material. West of the subduction zone, the Juan de Fuca Plate is sufficiently large and fast moving to influence mantle flow geometry. The Gorda Plate, however, is not. Flow directly beneath Gorda is instead induced by Pacific Plate motion. This places bounds on the size of plate capable of inducing asthenospheric flow.

Methods

Methods and any associated references are available in the online version of the paper.

Received 20 April 2015; accepted 25 September 2015; published online 2 November 2015

References

1. Conrad, C., Behn, M. & Silver, P. Global mantle flow and the development of seismic anisotropy: Differences between the oceanic and continental upper mantle. *J. Geophys. Res.* **112,** B07317 (2007).
2. Toomey, D. *et al.* The Cascadia initiative: A sea change in seismological studies of subduction zones. *Oceanography* **27,** 138–150 (2014).
3. Riddihough, R. Recent movements of the Juan de Fuca plate system. *J. Geophys. Res.* **89,** 6980–6994 (1984).
4. Eakin, C. *et al.* Seismic anisotropy beneath Cascadia and the Mendocino triple junction: Interaction of the subducting slab with mantle flow. *Earth Planet Sci. Lett.* **297,** 627–632 (2010).
5. Currie, C. *et al.* Shear wave anisotropy beneath the Cascadia subduction zone and western North American craton. *Geophys. J. Int.* **157,** 341–353 (2004).
6. Long, M. & Silver, P. The subduction zone flow field from seismic anisotropy: A global view. *Science* **319,** 315–318 (2008).
7. Silver, G. & Chan, W. Shear wave splitting and subcontinental mantle deformation. *J. Geophys. Res.* **96,** 16429–16454 (1991).
8. Nicolas, A. & Christensen, N. in *Composition, Structure and Dynamics of the Lithosphere-Asthenosphere System* (eds Fuchs, K. & Froidevaux, C.) 111–123 (Geodynamics Series 16, American Geophysical Union, 1987).
9. Karato, S., Katayama, I. & Skemer, P. Geodynamic significance of seismic anisotropy of the upper mantle: New insights from laboratory studies. *Ann. Rev. Earth Planet. Sci.* **36,** 59–95 (2008).
10. Song, T. & Kawakatsu, H. Subduction of oceanic asthenosphere: Evidence from sub-slab seismic anisotropy. *Geophys. Res. Lett.* **39,** L17301 (2012).
11. Heesemann, M. *et al.* Ocean Networks Canada: From geohazards research laboratories to Smart Ocean Systems. *Oceanography* **27,** 151–153 (2014).
12. Bell, S., Forsyth, D. & Ruan, Y. Removing noise from the vertical component records of ocean-bottom seismometers: Results from year one of the Cascadia Initiative. *Bull. Seismol. Soc. Am.* **105,** 300–313 (2014).
13. Webb, S. Broadband seismology and noise under the ocean. *Rev. Geophys.* **36,** 105–142 (1998).
14. Lodewyk, J. & Sumy, D. *Cascadia Amphibious Array Ocean Bottom Seismograph Horizontal Component Orientations* (OBSIP Management Office, 2014); http://www.obsip.org/experiments/experiment-list/2011/cascadia
15. Wolfe, C. & Solomon, S. Shear-wave splitting and implications for mantle flow beneath the MELT region of the East Pacific Rise. *Science* **280,** 1230–1232 (1998).
16. Fontaine, F. *et al.* Upper-mantle flow beneath French Polynesia from shear wave splitting. *Geophys. J. Int.* **170,** 1262–1288 (2007).
17. Zandt, G. & Humphreys, E. Toroidal mantle flow through the western US slab window. *Geology* **36,** 295–298 (2008).
18. Obrebski, M. *et al.* Slab-plume interaction beneath the Pacific Northwest. *Geophys. Res. Lett.* **37,** L14305 (2010).
19. Nishimura, C. & Forsyth, D. The anisotropic structure of the upper mantle in the Pacific. *Geophys. J. Int.* **96,** 203–229 (1989).
20. Kendall, J. *et al.* Magma-assisted rifting in Ethiopia. *Nature* **433,** 146–148 (2005).
21. Blackman, D. & Kendall, J. Sensitivity of teleseismic body waves to mineral texture and melt in the mantle beneath a mid-ocean ridge. *Phil. Trans. R. Soc. Lond. A.* **355,** 217–231 (1997).
22. Gripp, A. & Gordon, R. Young tracks of hotspots and current plate velocities. *Geophys. J. Int.* **150,** 321–361 (2002).
23. Debayle, E. & Ricard, Y. Seismic observations of large-scale deformation at the bottom of fast-moving plates. *Earth Planet. Sci. Lett.* **376,** 165–177 (2013).
24. Chaytor, J. *et al.* Active deformation of the Gorda plate: Constraining deformation models with new geophysical data. *Geology* **32,** 353–356 (2004).
25. Hager, B. H. & O'Connell, R. J. A simple global model of plate dynamics and mantle convection. *J. Geophys. Res.* **86,** 4843–4867 (1981).
26. Fjeldskaar, W. Viscosity and thickness of the asthenosphere detected from the Fennoscandian uplift. *Earth Planet. Sci. Lett.* **126,** 399–410 (1994).
27. Wessel, P. & Smith, W. New, improved version of Generic Mapping Tools released. *EOS Trans. Am. Geophys. Union* **79,** 579 (1998).
28. Wüstefeld, A. *et al.* Identifying global seismic anisotropy patterns by correlating shear-wave splitting and surface-wave data. *Phys. Earth Planet. Int.* **176,** 198–212 (2009).
29. Porritt, R., Allen, R. & Pollitz, F. Seismic imaging east of the Rocky Mountains with USArray. *Earth Planet. Sci. Lett.* **402,** 16–25 (2014).
30. Hayes, G., Wald, D. & Johnson, R. Slab1.0: A three-dimensional model of global subduction zone geometries. *J. Geophys. Res.* **117,** B01302 (2012).

Acknowledgements

Support for this work was provided by the National Science Foundation (OCE-1139701) to R.M.-S. and R.M.A. The data used in this research were provided by instruments from the Ocean Bottom Seismograph Instrument Pool (http://www.obsip.org), which is funded by the National Science Foundation under cooperative agreement OCE-1112722. The work benefited from discussions with J. Lodewyk, A. Frassetto and C. Eakin. GMT (Wessel and Smith[27]) and MATLAB were used to create the figures.

Author contributions

This study was carried out and written up by R.M.-S., under supervision of R.M.A. I.D.B. assisted with data analysis and helped write the paper. E.T. and M.A.R. provided advice and minor modifications to the text.

Additional information

Supplementary information is available in the online version of the paper. Reprints and permissions information is available online at www.nature.com/reprints. Correspondence and requests for materials should be addressed to R.M.-S.

Competing financial interests

The authors declare no competing financial interests.

Methods

Shear wave splitting. We determine the splitting parameters ϕ and δt for each station–event pair using Splitlab (ref. 31) and SHEBA (ref. 32). Splitlab uses three standard techniques: the rotation-correlation method (RC; ref. 33), the minimum energy method (SC; ref. 8) and the eigenvalue method (EV; ref. 8). This allows measurement classification as 'good', 'fair' or 'poor' according to the criteria of ref. 34. SHEBA uses the eigenvalue method alone and incorporates a cluster analysis algorithm, thus decreasing subjectivity in phase arrival picking[32]. A total of 631 'fair' or 'good' measurements were made and subsequently stacked using the method of ref. 35. This number includes high-quality null results, which occur where the anisotropy is very weak, or aligned parallel or perpendicular to the initial polarization of the seismic wave[34] (see Supplementary Sections 3 and 5 for more information). We used events with moment magnitudes greater than 6.0 and with epicentral distances of between 85° and 130°. Teleseismic SKS and SKKS phases were used because their passage through the core as P waves removes source-side anisotropic effects[7]. Given that the lower mantle is approximately isotropic, the main splitting signal source observed in teleseismic studies is likely to be within the upper 400 km of Earth structure, directly beneath the seismometers[7].

The short deployment time of the OBS stations and small number of high-quality splitting results obtained limit back-azimuthal coverage and make it difficult to model this data set with more than a single layer of anisotropy. Given this constraint, we chose not to include information about back-azimuth in the stacking process.

Shear wave splitting of OBS data is complicated by the potential for component misorientation (for example, ref. 14). This arises because OBS instruments settle on the seabed in unknown orientations that must be determined after recovery to rotate the horizontal components into the true 'east' and 'north' directions. The horizontal orientations of the Cascadia Initiative and X9 stations were determined using the surface wave polarization method of Stachnik[36]. The accuracy of the results was then checked during the splitting process by comparing initial polarization estimates to back-azimuth directions and ensuring separation of approximately 0° or 180°.

A further check on the orientations can be carried out by virtue of how the three methods respond to misaligned components[37]. It has been shown that EV and RC splitting time estimates are unaffected by component misorientation, whereas small inaccuracies in orientation introduce large errors for the SC method[37]. Our measurements were characterized as 'good' or 'fair' only when there was satisfactory agreement between the delay time predictions of the three methods. SC method results are reported singularly in this paper because this technique has been determined to be least sensitive to noise and exhibits the highest accuracy proximal to null measurements[34].

High levels of long-period noise are present in the OBS data[12,13]. Filtering was used to optimize noise reduction without unduly compromising the splitting measurements. The characteristic frequency of teleseismic SKS waves ranges between 0.08–0.13 Hz but most onshore studies use band-pass filters such as 0.02–0.20 Hz, which capture the full range of SKS energy[3,7]. The presence of strong 0.16–0.2 Hz secondary microseismic noise peaks in the OBS data[12], however, means that such filter bands are not typically useful in this case. OBS data are further affected by strong compliance noise ranging from 0.01–0.04 Hz, attributed to infragravity waves[11]. This suggests an optimal filter band close to the 'noise notch' of 0.03–0.1 Hz, as identified in ref. 13. Typically we choose a region of 0.05–0.15 Hz, but employ frequencies between 0.03 and 0.18 Hz on an event-by-event basis to optimize the signal-to-noise ratio. To limit subjectivity many events had their splitting parameters determined in multiple frequency bands and multiple time windows. Only events with signal-to-noise greater than 4.0 were used in the stack. Upper filter corner frequencies below 0.14 Hz were omitted to avoid signal energy reduction, which makes measurements seem increasingly null. For further details, see Supplementary Sections 2–5.

Geodynamic modelling. Our simple two-dimensional (2D) model of the mantle flow field beneath diverging plates was constructed as a test of our interpretation of the splitting geometry observed beneath the Gorda Plate. The propagator matrix method for 2D periodic flow given in the appendix of ref. 25 was used to solve for instantaneous, incompressible, Newtonian viscous (Stokes) flow with piecewise-constant horizontal (plate) motions imposed at the top of the mantle. Solutions are obtained in Fourier series form with periodic boundary conditions horizontally. To approximate the situation along a profile perpendicular to the Gorda Ridge, we model one plate as stationary while the other diverges at a constant speed (60 mm yr^{-1}). We focus on flow within a 400 km horizontal window centred at the velocity jump, and choose a horizontal periodic boundary condition whose fundamental length scale is much larger than this window length (Fig. 3, bottom panel). We follow ref. 38 by assuming a two-layer structure featuring a thin, low-viscosity and thick, underlying mantle layer. We base our viscosity contrast and layer thickness estimates (100 km and a viscosity contrast of 100) on the work of ref. 26, although we acknowledge that the width and viscosity of the asthenosphere is poorly constrained (Supplementary Section 10). Recent seismic constraints, especially seismic anisotropy studies beneath the Pacific Plate[39], suggest strongly that the base of the highly anisotropic asthenosphere is at approximately 200 km depth, which is consistent with geodynamic constraints as long as the viscosity contrast is at least 2–3 orders of magnitude[40]. Thus, our choice remains arbitrary, although the thickness and viscosity parameters we employ reflect the findings of recent studies. Our model extends to 660 km in depth, where the vertical flow field is set to zero at the bottom of the layer. Figure 3a shows our preferred model, where the asthenosphere viscosity is reduced by a factor of 100. The model does not account for complicated features such as the 3D plate geometry or the subduction zone, but clearly the weak asthenosphere causes flow to be induced immediately beneath the stationary plate that is strongly aligned with motion of the moving plate. We therefore propose that the large, fast-moving Pacific Plate induces asthenospheric flow beneath the small, fragmented, slow-moving Gorda Plate that is strongly aligned with Pacific Plate motion, as observed.

Data availability. The facilities of IRIS Data Services, and specifically the IRIS Data Management Center, were used for access to waveforms, related metadata, and/or derived products used in this study. IRIS Data Services are funded through the Seismological Facilities for the Advancement of Geoscience and EarthScope (SAGE) Proposal of the National Science Foundation under Cooperative Agreement EAR-1261681.

The DNA13 North American tomography model, which was used in the creation of Fig. 1, can be downloaded from http://seismo.berkeley.edu/~rallen/pub/2014porritt/data.php.

The high-resolution bathymetry/topography data set used in the creation of Supplementary Section 2A was obtained from http://www.gebco.net/data_and_products/gridded_bathymetry_data/gebco_30_second_grid.

Shear wave splitting measurements from previous studies were obtained from http://splitting.gm.univ-montp2.fr/DB.

We plan to add our new results to this database.

Code availability. The shear wave splitting software packages Splitlab and Sheba are publicly available: The version of Splitlab used in this project can be downloaded from https://robporritt.wordpress.com/software. Sheba can be downloaded from https://github.com/jwookey/sheba. The code used to orient the OBS instruments can be obtained from http://www.obsip.org/data/obs-horizontal-orientation. We have opted not to make the code associated with our geodynamic modelling study available because it is tailored to a very specific situation and more generic software based on the method of ref. 25 is already widely available. However, we would be happy to provide our code if requested by email.

References

31. Wüstefeld, A. *et al.* SplitLab: A shear-wave splitting environment in Matlab. *Comp. Geosci.* **34,** 515–528 (2008).
32. Wüstefeld, A. *et al.* A strategy for automated analysis of passive microseismic data to image seismic anisotropy and fracture characteristics. *Geophys. Prospect.* **58,** 755–773 (2010).
33. Bowman, J. & Ando, M. Shear-wave splitting in the upper-mantle wedge above the Tonga subduction zone. *Geophys. J. Int.* **88,** 25–41 (1987).
34. Wüstefeld, A. & Bokelmann, G. Null detection in shear-wave splitting measurements. *Bull. Seism. Soc. Am.* **97,** 1204–1211 (2007).
35. Wolfe, C. & Silver, P. Seismic anisotropy of oceanic upper mantle: Shear wave splitting methodologies and observations. *J. Geophys. Res.* **103,** 749–771 (1998).
36. Stachnik, J. *et al.* Determination of New Zealand ocean bottom seismometer orientation via Rayleigh-wave polarization. *Seism. Res. Lett.* **83,** 704–713 (2012).
37. Tian, X. *et al.* SKS splitting measurements with horizontal component misalignment. *Geophys. J. Int.* **185,** 329–340 (2011).
38. Richards, M. *et al.* Role of a low-viscosity zone in stabilizing plate tectonics: Implications for comparative terrestrial planetology. *Geochem. Geophys. Geosyst.* **2,** 1026 (2001).
39. Nettles, M. & Dziewński, A. Radially anisotropic shear velocity structure of the upper mantle globally and beneath North America. *Geophys. J. Int.* **113,** B02303 (2008).
40. Paulson, A. & Richards, M. On the resolution of radial viscosity structure in modeling long-wavelength postglacial rebound data. *Geophys. J. Int.* **179,** 1516–1526 (2009).